# Is There Scaling in High-Reynolds-Number Turbulence?

Katepalli R. SREENIVASAN*) and Brindesh DHRUVA**)

*Mason Laboratory, Yale University, New Haven, CT 06520-8286, U. S. A.*

(Received November 5, 1997)

Turbulence velocity measurements have been made in the surface layer of the atmosphere at Taylor microscale Reynolds numbers between 10,000 and 20,000. Even at these high Reynolds numbers, the structure functions do not scale unambiguously. It is shown that the scaling improves significantly by implementing a plausible correction due to the mean shear. For second and fourth order structure functions, the exponents for the corrected data are close to those determined by extended self-similarity (ESS). ESS improves scaling enormously for all orders, and is used to obtain exponents for moment orders between $-0.08$ and 10. Anomaly prevails even for very low orders. A major qualitative conclusion is that it is difficult to discuss the scaling effectively without first understanding quantitatively the effects of finite shear and finite Reynolds numbers.

## §1. Introduction

Fully turbulent flows consist of a wide range of coupled scales which are classified, somewhat loosely, into "large" and "small" scales. The large scales are of the order of the flow width, contain most of the energy and dominate the transport. The small scales include the dissipative range and the inertial range; the latter are large compared to dissipative scales but small compared to the large scales. The notion of universality is generally associated with Kolmogorov,[1] its principal originator, and often designated as K41 for short. According to K41, the moments of velocity increments, or the so-called longitudinal structure functions, obey the relation

$$\langle \Delta u_r^n \rangle = C_n (r\langle \varepsilon \rangle)^{n/3}, \tag{1}$$

where $u$ is the turbulent velocity fluctuation in the longitudinal direction $x$, $\Delta u_r = u(x+r) - u(x)$, $r$ is the separation distance in the direction $x$, $\langle \varepsilon \rangle$ is the mean rate of energy dissipation, $n$ is a positive integer and $C_n$ are universal constants. A similar equation can be written for velocity increments with the separation distance transverse to the direction of the velocity component.

Of these structure function relations, an exact relation is known only for the third order.[2] This so-called Kolmogorov $\frac{4}{5}$-ths law is given for the inertial range by

$$\langle \Delta u_r^3 \rangle = -\frac{4}{5} r \langle \varepsilon \rangle. \tag{2}$$

Kolmogorov derived this result for globally homogeneous and isotropic turbulence. Since the equation involves only velocity differences, it is thought that it might be exact for all types of flows if only local homogeneity and isotropy holds. The demands

*) E-mail address: k.sreenivasan@yale.edu

**) E-mail address: brindesh.dhruva@yale.edu

on global isotropy can be relaxed,[3] but not, apparently, the assumption of global homogeneity.

It is now believed[4] that Eq. (1), and thus the K41 universality, does not hold. It is thought, instead, that

$$\langle \Delta u_r^n \rangle \sim r^{\zeta_n}, \tag{3}$$

where it is presumed that the $\zeta_n$ are universal but the unspecified prefactors are non-universal. Many experimental studies have been made purporting to show that the $\zeta_n$ in Eq. (3) are different from $n/3$ and are anomalous (that is, $\zeta_{2n} \neq 2 \times \zeta_n$).

Unfortunately, the experimental determination of $\zeta_n$ is not fully satisfactory. The first and obvious requirement for obtaining exponents unambiguously is the presence of a wide scaling range. It is generally thought that the extent of the scaling range increases as a power of the Reynolds number. However, the scaling range depends, besides the Reynolds number, quite strongly on the nature and strength of forcing.[5] It appears that the cleanest flow to study from the perspective of scaling is one in which the forcing is mild and occurs in a very narrow scale range. Given that many experiments do not satisfy this criterion and show ambiguous scaling, various self-consistent — but debatable — schemes have been used to determine the exponents.

One procedure is to plot the Kolmogorov function $K(r) \equiv \langle \Delta u_r^3 \rangle / r \langle \varepsilon \rangle$ as a function or $r$ and fix the scaling range as that over which $K(r) = \frac{4}{5}$. First, for $K$ to reach this value, one requires a Taylor microscale Reynolds number of the order of a few hundreds.[5] Even then, unless the Reynolds number is truly large, there is no scale range for which $K$ is strictly flat. Its typical shape is shown in Fig. 1; also shown is the presumed scaling range. This is then fixed for structure functions of all orders, and exponents are obtained by least-square fits to the data within that range. This procedure was first employed in Ref. 6), and later by others as well. Even in the high-Reynolds-number helium experiments of Ref. 7), the situation is not far better.

All measurements using this procedure have yielded a set of numbers for the exponents which differ from $n/3$. Different flows seem to yield slightly different numbers, but the uncertainties in the determination of the scaling range, the least-square errors, and so forth, are large enough that one cannot be certain that the differences among the flows are genuine. One thus clings to the notion of universal exponents.

There is no rationale for keeping the scaling range unchanged for all orders of structure functions. Its chief merit is its self-consistency. Other self-consistent procedures can be rationalized. For example, one could require that the inner cut-off for the $n$-th order structure function be set at a scale $\eta_n$ such that the Reynolds number

$$R_i \equiv \langle |\Delta u_r|^n \rangle^{1/n} \eta_n / \nu = \langle \Delta u_r^3 \rangle^{1/3} \eta_3 / \nu, \tag{4}$$

where $\eta_n$ is the lower cut-off for the $n$-th order structure function, and $\eta_3$ is determined as above. The thinking here is that the inertial range begins at a scale for which $R_i$ assumes the value determined from the third-order — not at a fixed multiple of the Kolmogorov scale for all moment orders, as implied previously. This

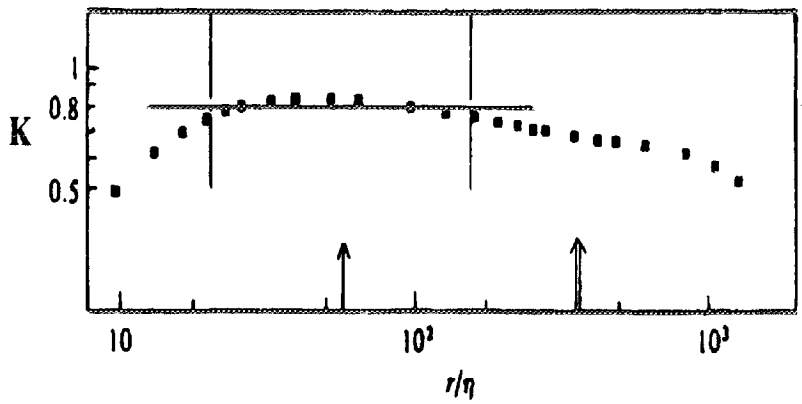


Fig. 1. A typical plot of the Kolmogorov function $K$ in the jet experiments of Ref. 6); $R_\lambda = 852$. $K$ is not strictly flat anywhere, so the scaling region is thought to correspond to the part where the deviations from constancy are "not too large". The vertical lines are chosen to be those limits. These limits are fixed to be the same for all high-order structure functions. The procedure has been followed by a number of researchers since then. For reference, the Taylor microscale $\lambda$ is shown by the single arrow; the double arrow indicates $\frac{1}{4}L$, where $L$ is a suitably defined integral scale.

moves the inner cut-off to slightly lower values for higher order moments. A corresponding rationale for setting the upper cut-off is unclear, but one may set it at the same fraction of the integral scale as for the third-order structure function. The net outcome is that the exponents become marginally bigger. However, unless the flow Reynolds number is immense, the modifications are well within the uncertainty of measurements, and so one is again led to the conclusion that the anomaly survives.[8)]

A slightly more sophisticated procedure comes from the realization that the power-law part of the structure functions is only asymptotic, and that the inner and outer scales will have finite effects at all finite Reynolds numbers. To this end, if one had a theory for the scaling function — by which is meant an analytic form for structure functions that not only exhibits the asymptotic power-law but also the trend towards the power-law — one could determine the exponents with greater confidence. At present, there is no such theory. There is a useful interpolation formula[9)] for second-order statistics, which has been extended to high-order moments in Ref. 10). These formulae apply down to the smallest scales, thus increasing the range of scales available for least-square fits. Firmer values for the exponents can thus be obtained. They are anomalous as well,[10)] quite close to those obtained by earlier methods. However, the "scaling function" is not based on a formal theory, so the method is not exact.

Yet another intriguing procedure[11)] is as follows. Inserting Eq. (2) in Eq. (3), one may write

$$\langle \Delta u_r^n \rangle \sim \langle \Delta u_r^3 \rangle^{\zeta_n}. \tag{5}$$

Since all structure functions have roughly the same shape, plotting one against the other generally yields a somewhat more extensive scaling range and allows a more confident determination of the exponents. This procedure is called extended self-

similarity (ESS). In practice, one replaces Eq. (4) by

$$\langle \Delta u_r^n \rangle \sim \langle |\Delta u_r|^3 \rangle^{\zeta_n} \tag{6}$$

without much justification, but it does not seem to produce any qualitative differences because, empirically, $\langle |\Delta u_r|^3 \rangle \sim \langle \Delta u_r^3 \rangle^{1.05}$ to an excellent approximation. Even though the procedure works less well for sheared flows,[12] it produces a significant improvement.

In summary, there exists no measurement until now that displays completely convincing scaling over an acceptably large scaling range. Thus, one is forced to invent several self-consistent procedures to estimate the exponents with greater confidence. All such estimates display anomaly. The open question is whether these estimates are equivalent to the theoretical exponents defined in Eq. (3), or suffer from systematic and procedure-dependent artifacts.

## §2. Experiments

Motivated by these considerations, we have made a series of measurements in atmospheric turbulence at Taylor microscale Reynolds numbers ranging between 10,000 and 20,000. These Reynolds numbers are comparable to the highest ever used for studies of the small-scale (e.g., Ref. 13)). The usual procedure of surrogating time for space ("Taylor's hypothesis") was used, but we have made a few tests to convince ourselves that this is not a critical factor. The tests involved a few comparisons with true spatial data obtained simultaneously from two probes separated by known streamwise distances.

The velocity data were acquired by means of single-wire and ×-wire probes mounted at a height of about 35 m above the ground on a meteorological tower at the Brookhaven National Laboratory. The hot-wires were about 0.7 mm in length and 6 $\mu$m in diameter. They were calibrated just prior to mounting them on the tower (and checked immediately after dismounting), and operated on DISA 55M01 constant-temperature anemometers. The frequency response of the hot-wires was typically good up to 20 kHz. The voltages from the anemometers were low-pass filtered and digitized. The low-pass cut-off was never more than half the sampling frequency, $f_s$. The voltages were constantly monitored on an oscilloscope to ensure that they did not exceed the digitizer limits. Also monitored were on-line spectra from an HP 3561A Dynamic Signal Analyzer. The wind speed and direction were independently monitored by a vane anemometer mounted close to the tower. The voltages were converted to velocities in a standard way through the calibration procedure. The mean wind velocities, roughly constant over the duration of a given data set, ranged between 5 and 10 $\text{ms}^{-1}$ in the experiment series. The Kolmogorov scale, $\eta$, varied between 0.44 and 0.64 mm among the various data sets. The real-time duration of data records was typically of the order 2500 sec. Table I lists a few relevant facts for the data records analyzed here.

Figure 2 shows the spectral density, $E_{11}(\kappa_1)$, for the velocity fluctuation, plotted against the wavenumber $\kappa_1$ (obtained via Taylor's hypothesis, using the mean velocity $\overline{U}$). The spectra are computed by splitting the long signal into smaller segments,

Table I. Basic information about the data records analyzed in this paper. Here, the various symbols have the following meanings: $\overline{U}$ = local mean velocity, $u'$ = root-mean-square velocity, $\langle\varepsilon\rangle$ = energy dissipation obtained by the assumption of local isotropy and Taylor's hypothesis, $\eta$ and $\lambda$ are the Kolmogorov and Taylor length scales, respectively, the microscale Reynolds number $R_\lambda \equiv u'\lambda/\nu$, and $f_s$ is the sampling frequency.

| $\overline{U}$ $ms^{-1}$ | $u'$ $ms^{-1}$ | $\langle\varepsilon\rangle$ $m^2s^{-3}$ | $\eta$ mm | $\lambda$ cm | $R_\lambda$ | $f_s$, per channel, Hz | number of samples |
|---|---|---|---|---|---|---|---|
| 7.6 | 1.36 | $3.2 \times 10^{-2}$ | 0.57 | 11.4 | 10,340 | 5,000 | $10^7$ |
| 4.8 | 1.45 | $2.0 \times 10^{-2}$ | 0.64 | 15.4 | 14,860 | 2,000 | $5 \times 10^6$ |
| 8.3 | 2.30 | $7.8 \times 10^{-2}$ | 0.45 | 13.0 | 19,500 | 5,000 | $4 \times 10^7$ |
| 5.2 | 1.80 | $0.92 \times 10^{-2}$ | 0.44 | 8.9 | 10,670 | 5,000 | $4 \times 10^7$ |

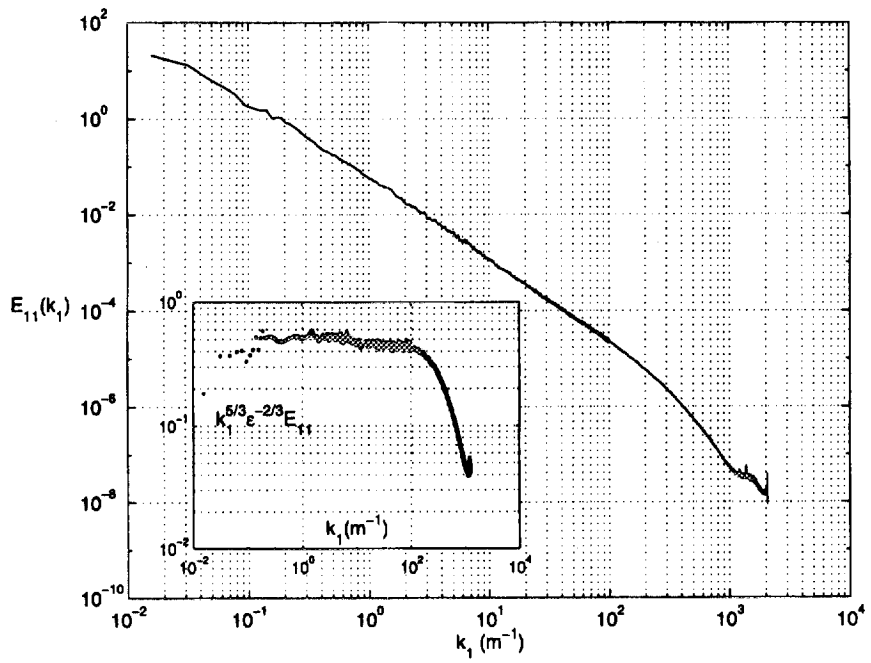


Fig. 2. The longitudinal spectral density, $E_{11}(\kappa_1)$, as a function of the longitudinal component of the wavenumber, $\kappa_1$. The first data set in Table I has been used. Taylor's hypothesis has been used for converting frequency to wavenumber. The inset shows the compensated spectrum according to K41.

which are processed through a standard FFT routine and ensemble averaged. The lowest wavenumber shown on the spectra is limited by the length of the segments used for FFT, *not* by the length of the record. Spectral scaling appears to exist for over three decades. The inset shows $\kappa_1^{5/3}E_{11}(\kappa_1)$, which is the spectral density compensated according to K41.

## §3. Two concerns

Figure 3 shows the Kolmogorov function $K \equiv \langle \Delta u_r^3 \rangle / r \langle \varepsilon \rangle$ as a function of spatial separation distance $r$ (normalized by $\eta$). The flat part of $K$ is not far from 0.8, as expected from the $\frac{4}{5}$-ths law. Loosely speaking, a scaling region for about two decades could be inferred. It appears measurably smaller than that inferred from the spectral density. Similarly, if one plots the second and fourth order structure functions against the scale separation $r$, regions of plausible scaling do appear (Figs. 4(a) and (b)).

However, one runs into difficulties if one attempts to define the scaling range more precisely by computing the local slopes of $K$ and other structure functions. For the former, one finds — at best — a small region about half-a-decade or so in extent (inset to Fig. 3). This is not large enough for a precise evaluation of the exponents. For second and fourth order exponents, insets to Figs. 4(a) and (b) show that there are no clean scaling regions. If the situation is only this good at $R_\lambda$ of 19,500, what can be said of turbulence at much smaller $R_\lambda$? How can one say with any confidence there is scaling in turbulence, let alone determine the exponents with certainty?

A second concern is the following. For universal exponents to exist, all inertial range statistics obtained by conditioning on the large scale must be independent of the large scale; or, if a dependence were to be observed, it should occur in some universal way. In Ref. 15), it was shown that the inertial-range conditional statistics

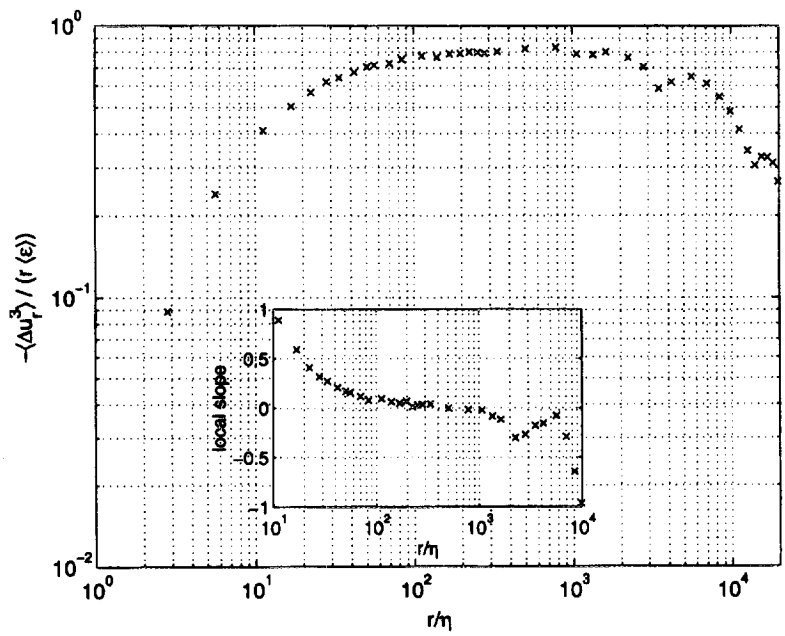


Fig. 3. The Kolmogorov function $K$ for the present atmospheric data (for the first data set in Table I). It appears that the scaling range is quite extensive (although substantially smaller than in Fig. 2). The inset indicates the local slope, obtained by finite difference approximation of $K$. Interpreted blindly, the inset suggests that the scaling range is no more than half-an-order of magnitude in extent, corresponding to the region where the local slope is close to zero.

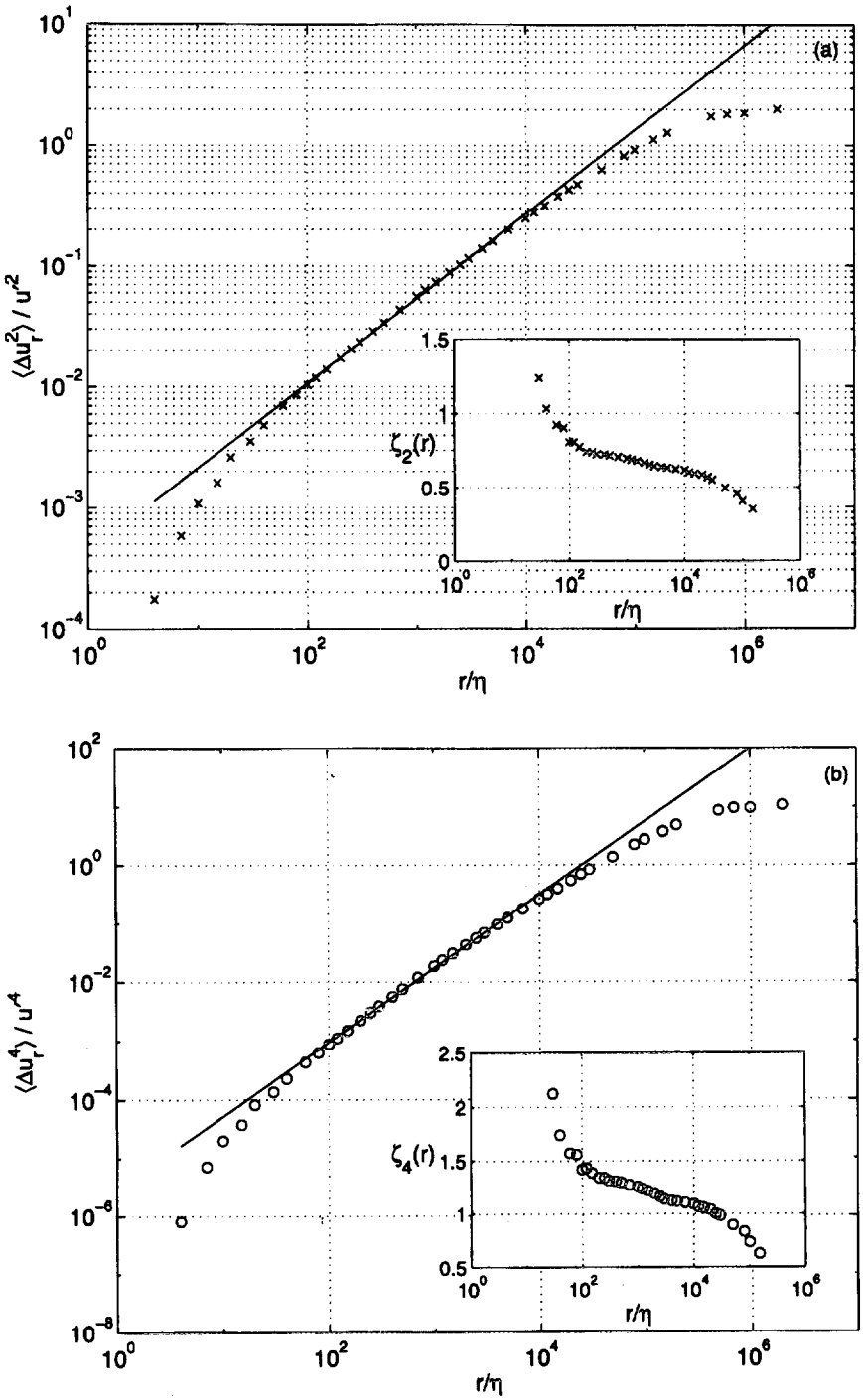


Fig. 4. (a) The second-order structure function (normalized by the mean square velocity) as a function of $r$. At first sight, it would appear that there is an ample scaling region (shown by a line of constant slope of 0.71), but the local slope (see inset) reveals that this is not the case. (b) shows similar data for the fourth-order structure function. The conclusions are also similar. The line has a slope of 1.28. The third set of data of Table I has been used.

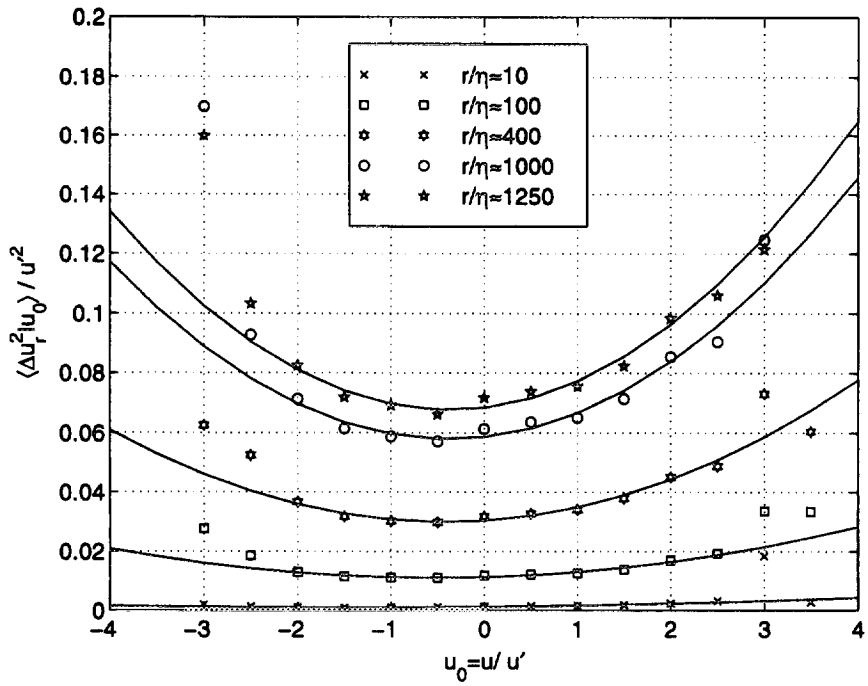


Fig. 5. The conditional expectation of $\Delta u_r^2$, conditioned on the large-scale velocity $u_o$, plotted as a function of $u_o$. Each symbol corresponds to a different separation distance $r$ (defined by the time interval $\Delta t = \frac{r}{U+u_o}$). Here and in other figures, $u_o$ is taken as the velocity at the middle of the interval $(x, x+r)$, but other definitions of $u_o$ (for instance, as the average of the velocity at the endpoints of the interval) make little difference. The first and second sets of data have been combined. The lines are the least-square fits of Eq. (7) to the data between $-2$ and $+2$ standard deviations. Similar conditional statistics for the fourth-order structure function reveal the same qualitative behavior, and can also be approximated by Eq. (7) with a different set of coefficients. In the second reference cited in Ref. 15), it has been shown that the energy dissipation, when conditioned on the large scale, shows a qualitatively similar dependence.

do depend on the large-scale. Figure 5 illustrates this feature: the quantity $\langle \Delta u_r^2 | u = u_o \rangle$ shows a strong dependence on the large-scale velocity $u_o$, when $u_o$ is large. On the other hand, the situation for homogeneous and isotropic turbulence is quite different, as can be seen for the DNS data[14] (see Fig. 6(a)) and for the grid turbulence data obtained using a standard set-up in the wind tunnel (see Fig. 6(b)). It is true that the Reynolds numbers in these latter two cases are small in comparison to the atmospheric data. However, if the large-scale effect did persist in the isotropic case, it would have been stronger at these low Reynolds numbers. We may therefore conclude that the inertial-range quantities show no dependence on the large scale in isotropic turbulence. The fact that the large-scale effects are present in shear flows (and are not universal), and that they are non-existent in shear-free isotropic case, demands that one will have to understand the effects of shear on scaling.

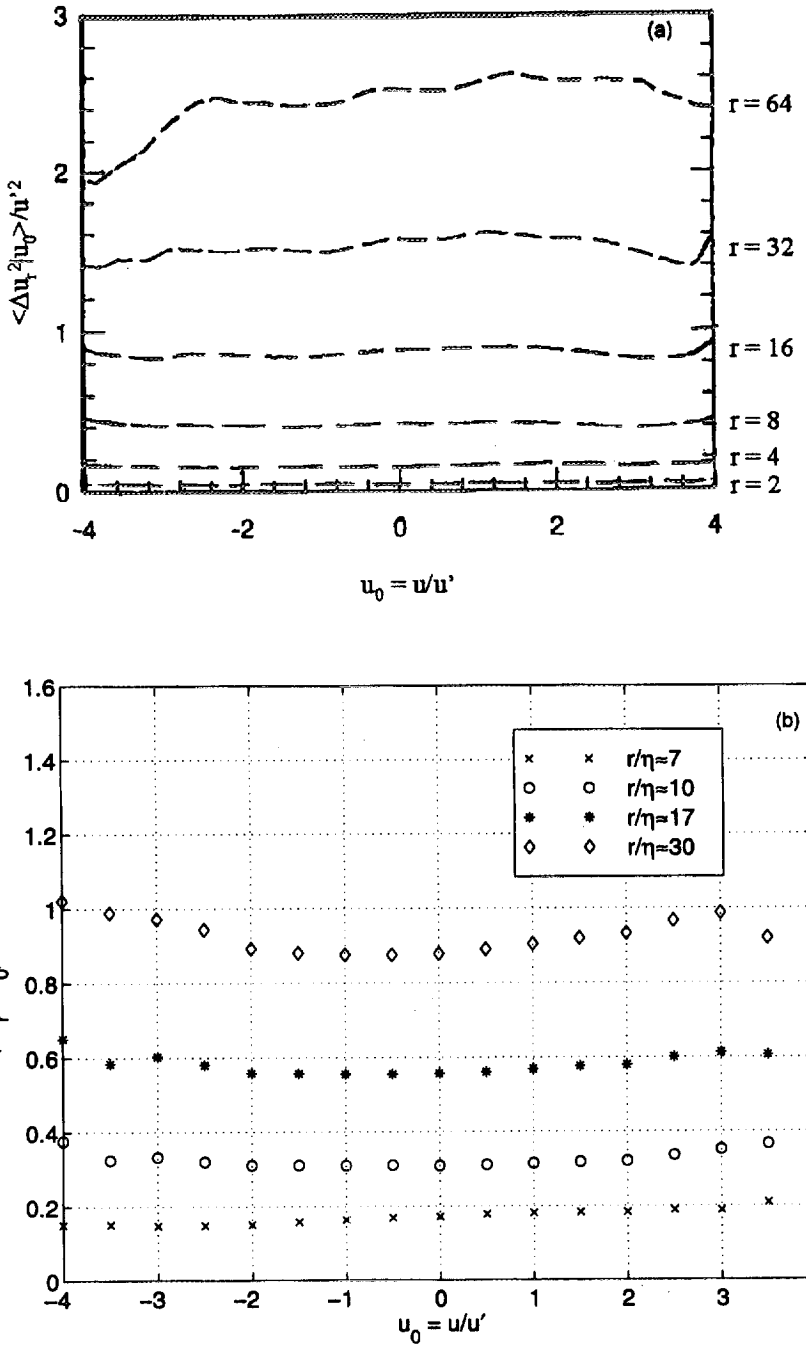


Fig. 6. (a) The same conditional statistics as in Fig. 5, for the DNS data for isotropic turbulence in a periodic box.[14] The Taylor microscale Reynolds number $R_\lambda = 210$. Different curves correspond to different values of the (true spatial) separation distance $r$, marked in units of the mesh length. (b) shows the same quantities for the grid-turbulence data. These were obtained at a streamwise distance of 52 cm behind a square mesh grid of mesh size 1.27 cm. The mean velocity was 12 $ms^{-1}$, $R_\lambda = 60$. In both (a) and (b), unlike in Fig. 5, the inertial range conditional statistics do not show a perceptible dependence on the large scale velocity. Taylor's hypothesis was used in (b).

## §4. Effects of shear and viscous cut-off

It is worth stressing that Eq. (2) is an asymptotic expectation and that, at any finite Reynolds number, the effects of the viscous scales and the large scales might be felt in the inertial range. Without understanding these 'corrupting' effects on scaling, the insistence on computing the local slopes is a misplaced delusion. The extent of these corrupting influences is not known theoretically. Here, we discuss them at a certain semi-empirical level.

For this purpose, let us return to Fig. 5 where the conditional variance of $\Delta u_r$ for fixed $u_o$ is given as a function of $u_o$ for several values of $r$. It is useful to fit the data of Fig. 5 roughly by second-order parabola

$$\langle \Delta u_r^2 | u = u_o \rangle = a_2 + b_2 u_o + c_2 u_o^2, \tag{7}$$

where the dependence of the constants $a_2$, $b_2$ and $c_2$ on the separation distance $r$ is suppressed for simplicity. The quality of fits is less than perfect for large $u_o$, but can be improved by using a higher-order polynomial in $u_o$. This does not change the situation much, and the issue can be illustrated quite adequately by the second-order fit. Similar fits have been obtained for the fourth-order conditional average.

We now make use of the identity

$$\langle \Delta u_r^n \rangle = \int_{-\infty}^{\infty} \langle \Delta u_r^n | u = u_o \rangle p(u_o) du_o, \tag{8}$$

where $n$ is either 2 or 4, and $p(u_o)$ is the probability density function of the large-scale velocity $u_o$. Combining Eqs. (7) and (8), one obtains

$$\langle \Delta u_r^n \rangle = a_n(r) + c_n(r) \langle u_o^2 \rangle. \tag{9}$$

The $b_n$ terms drop out because the mean of $u_o$ is zero; in any case, $p(u_o)$ is symmetric (see Fig. 7) which will render all odd-order terms zero in any high-order polynomial fit to conditional statistics. The second term in the above equation would be absent if the dependence on $u_o$ were absent; we would then be left with just the part that is independent of the large scale. The large-scale dependence can be expressed explicitly as a shear effect by rewriting the second term in Eq. (9) as

$$c_n' \frac{\langle u_o^2 \rangle}{\langle \varepsilon \rangle} \left| \frac{dU}{dy} \right|,$$

where $dU/dy$ is the shear (gradient of the mean velocity) and the prefactor $c_n'$ is redefined suitably. The rationale for introducing the shear is that the second term would be zero without the mean shear; the rationale for introducing the absolute value of the shear is the experience that the sign of the shear makes no difference to the large-scale dependence.

We can thus separate the $r$ dependence of structure functions in a shear flow into two parts; the first term in Eq. (9) is the shear-free part and the second term is due to the shear. It is useful to examine the scaling of the two terms separately. Figure 8(a) shows $a_2$ and $a_4$ as functions of $r$ for the atmospheric data. The inset

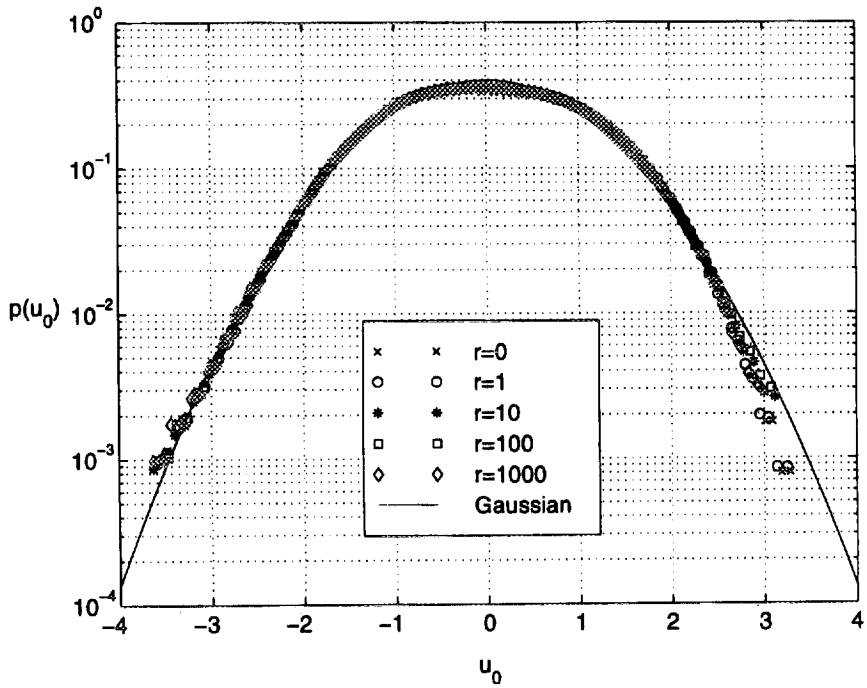


Fig. 7. The probability density function (pdf), $p(u_o)$, of the large-scale velocity $u_o$, plotted in the logarithmic coordinate. The crosses correspond to the definition of $u_o$ as the velocity at the mid-point of the separation interval (that is, the pdf is the same as that of the velocity fluctuation). Other symbols correspond to the cases where $u_o$ is defined as the average velocity between the endpoints of the separation interval. The different definitions do not produce any perceptible difference in the pdf. The pdf is symmetric (the skewness is $-0.03$) but not strictly Gaussian (the flatness factor is 2.66). The first and second sets of data from Table I have been combined. The full line is Gaussian with zero mean and unity standard deviation.

shows the local slopes. It is clear, in comparison with the local slopes of Figs. 4(a) and (b), that a qualitative improvement has been achieved. This now enables scaling exponents to be obtained with less ambiguity.

Let us now plot the ratios $c_2/a_2$ as well as $c_4/a_4$ as functions of $r$. Figure 8(b) shows that two ratios are small compared to unity. To a rough approximation, they are constants in $r$. These two facts suggest, first, that the effects of the large-scale on the scaling properties are small and, second, that the shear does not affect the scaling exponent itself (because $c_n$ scales roughly the same way as $a_n$). The dominant effect of the shear occurs in the prefactor. We may then conclude that the expectation of universal exponents is justified to a good approximation, but that the prefactors are large-scale dependent. However, a closer look suggests that the ratios $c_n/a_n$ are not exactly constants, so that some degree of corruption of scaling due to the $c_n$ term is expected. It is this feature that improves scaling when the $c_n$ term is removed. The scaling exponents determined from the $a_n$ are indeed anomalous ($\zeta_2 = 0.71$ and $\zeta_4 = 1.28$).

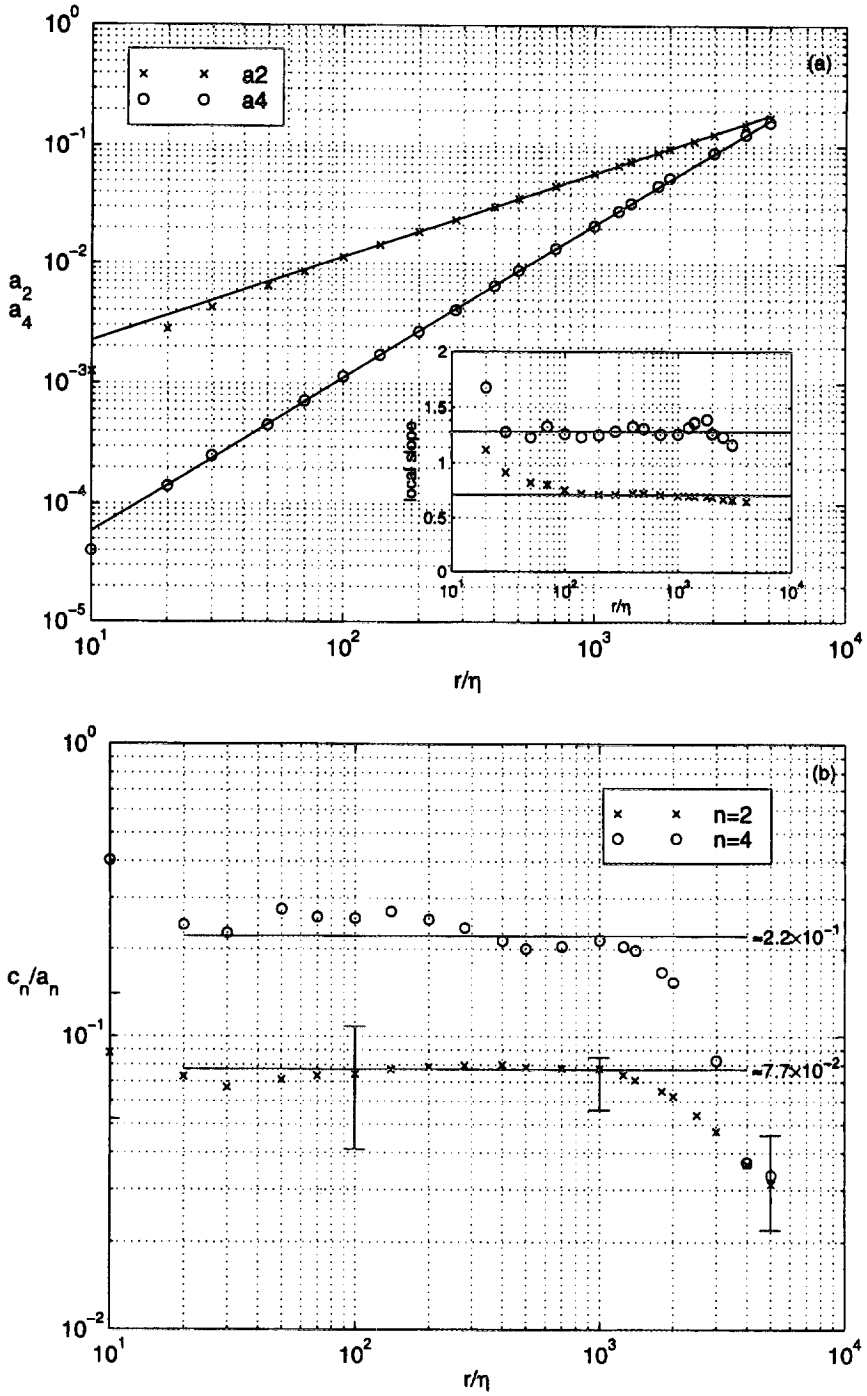


Fig. 8. (a) The scaling behavior of the shear-free parts $a_2$ and $a_4$. The local slopes are clearly suggestive of scaling. $\zeta_2 \approx 0.71$ and $\zeta_4 \approx 1.28$. (b) shows the ratios $c_2/a_2$ and $c_4/a_4$. The first and second sets of data from Table I have been combined.

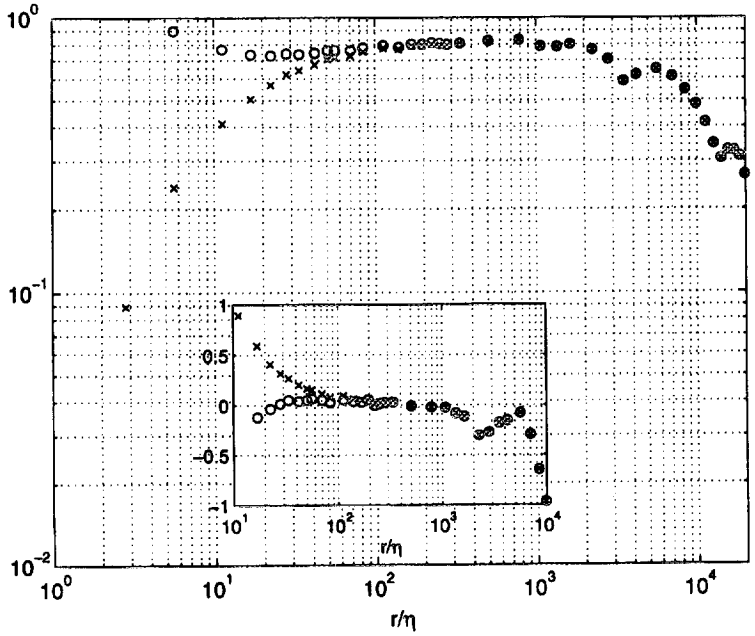


Fig. 9. The Kolmogorov function, $K$ (crosses), and $K$ after viscous corrections have been applied, according to Eq. (10) (circles). The local slope of the corrected form, plotted also as circles in the inset, shows a more extensive region where the Kolmogorov function is a constant.

An equally important effect is that of the viscous scale propagating into the inertial range. Let us examine this issue in the context of the third-order structure function, for which — at least for homogeneous turbulence — we know the full equation to be [2)]

$$\langle \Delta u_r^3 \rangle - 6\nu \frac{d\langle \Delta u_r^2 \rangle}{dr} = -\frac{4}{5}\langle \varepsilon \rangle r, \tag{10}$$

where the second term on the left side is the viscous correction. When the viscous correction is implemented, it is clear from Fig. 9 that better scaling than that of Fig. 3 is observed. Corrections expected from the large scales, not included in Eq. (10), can be accommodated somewhat similarly to those for the second and fourth order structure functions, but this will not be attempted here.

On the whole, these considerations show that the shear effects and cut-off effects corrupt scaling to various degrees. If these 'corrections' can be identified and extracted, as illustrated for a few cases here, it appears that an extensive scaling region could be observed for structure functions. Unfortunately, one does not quite know how to account for the effects formally correctly (except the viscous-scale effects for the third-order); the present work (see also Ref. 10)) constitutes no more than a useful beginning.

## §5. Scaling exponents from ESS

The exponents determined in the previous section for the second and fourth-order structure functions, after removing the shear effects, are very close to those determined by the ESS method. Exactly why the ESS method works is not fully understood (see, for example, Ref. 16)), but there is no doubt that the scaling improves measurably. This can be seen in Fig. 10 where the local slopes from ESS have been plotted for the second and fourth order structure functions. There is little ambiguity in obtaining the scaling exponents from here. It is possible that these exponents could differ from the $\zeta_n$ of Eq. (3). We have already mentioned that $\zeta_2$ and $\zeta_4$, determined after shear effects were removed, agree well with the ESS data. We thus tend to think that all other ESS exponents may be similarly close to the $\zeta_n$. For this reason, we have made a systematic study of the ESS exponents. Table II lists these exponents. Figure 11 compares them with K41. It is clear that the exponents are anomalous, as has been believed since the pioneering measurements of Ref. 6).

One result to which attention should be drawn is that even the very low-order exponents are anomalous (see inset to Fig. 11). This has already been noted in Ref. 18). (Note that for all non-integer orders of structure functions, we use the absolute

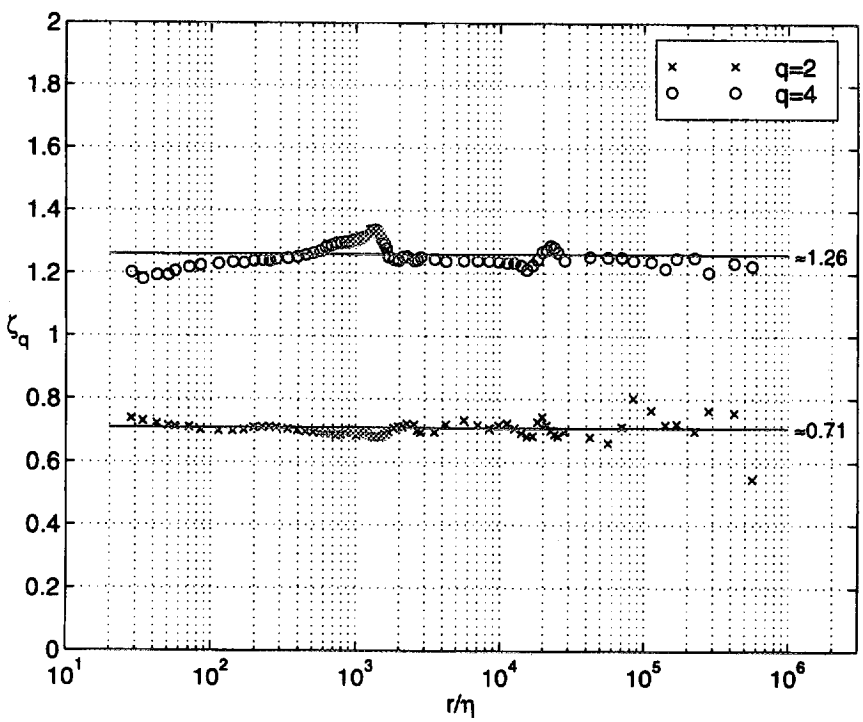


Fig. 10. Local slopes in the ESS plots for the second and fourth order structure functions. Both $\langle \Delta u_r^2 \rangle$ and $\langle \Delta u_r^4 \rangle$ were plotted against $\langle |\Delta u_r|^3 \rangle$ and the local slopes $\frac{d\langle \Delta u_r^n \rangle}{d\langle |\Delta u_r|^3 \rangle}$ were obtained. These slopes were converted to $\frac{d\langle \Delta u_r^n \rangle}{dr}$ using the unique relation between $\langle |\Delta u_r|^3 \rangle$ and $r$. The first set of data in Table I was used.

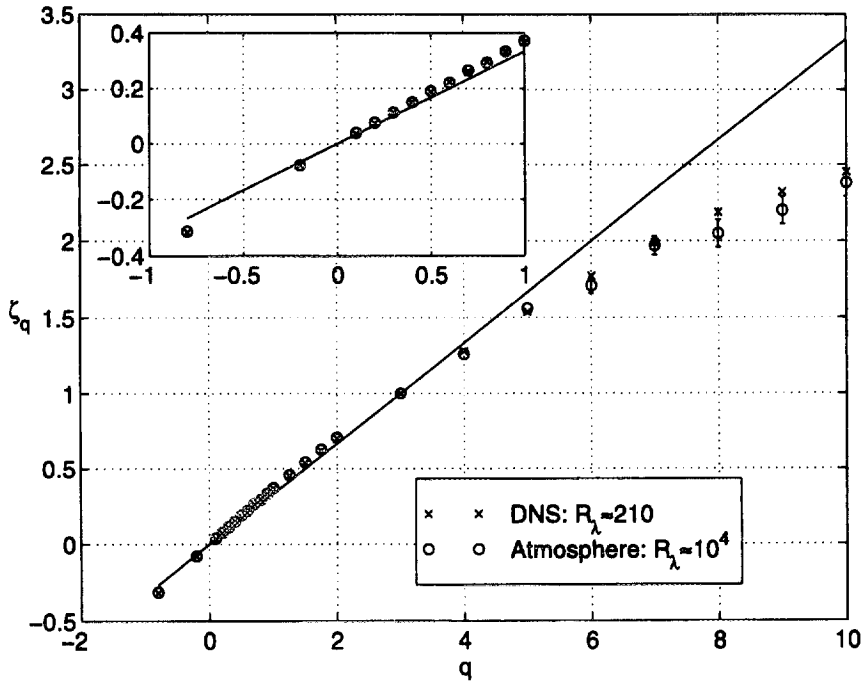


Fig. 11. ESS exponents for moment orders up to 10. Moment orders up to 6 converged well, but the numbers for higher orders are somewhat uncertain. Inset shows the exponents for low-order moments. The error bars for the numerical data are small and can be found in Ref. 17), from where they have been taken.

values of velocity increments.)

## §6. Concluding remarks

We have made a case that, despite some problems due to finite Reynolds numbers and finite shear, inertial range scaling does exist in high-Reynolds-number turbulence. To be able to see the scaling clearly, one has to understand these effects well. We have made a beginning for understanding the shear effects. Their removal allows the scaling exponents to be determined with greater certainty. We have not followed this through for exponents of all orders (because obtaining converged conditional data for high-order moments is rather difficult) but, on the basis of what we have studied, argue that the ESS exponents are close to the true exponents. We have obtained the former quite reliably.

Two further points need to be made. First, one of the advantages of ESS is that it can be applied to low Reynolds number data as well. This allows the determination of the Reynolds-number effects on ESS exponents. As an example, Fig. 12 plots the sixth-order exponent. This quantity decreases from a high value of about 2 to about 1.72, which appears to be the asymptotic value of $\zeta_6$. It might at first seem surprising that the value attained at the low-Reynolds-number end is close to K41. This may partly be an artifact of the ESS method because, at low Reynolds numbers, the

Table II. Scaling exponents from ESS ($R_\lambda = 10, 340$) compared with those for isotropic turbulence from the DNS data. Typical experimental error bars are shown on Fig. 11. The error bars on the DNS data can be found in Ref. 17) from where the exponents have been taken. They are quite small.

| order of moment | DNS exponents | present exponents |
|---|---|---|
| −0.80 | −0.317 | −0.313 |
| −0.20 | −0.077 | −0.078 |
| 0.10 | 0.036 | 0.039 |
| 0.20 | 0.073 | 0.076 |
| 0.30 | 0.112 | 0.113 |
| 0.40 | 0.150 | 0.150 |
| 0.50 | 0.187 | 0.190 |
| 0.60 | 0.223 | 0.221 |
| 0.70 | 0.260 | 0.265 |
| 0.80 | 0.296 | 0.292 |
| 0.90 | 0.332 | 0.333 |
| 1 | 0.366 | 0.372 |
| 1.25 | 0.452 | 0.458 |
| 1.50 | 0.536 | 0.542 |
| 1.75 | 0.619 | 0.628 |
| 2 | 0.699 | 0.708 |
| 3 | 1 | 1 |
| 4 | 1.279 | 1.26 |
| 5 | 1.536 | 1.56 |
| 6 | 1.772 | 1.71 |
| 7 | 1.989 | 1.97 |
| 8 | 2.188 | 2.05 |
| 9 | 2.320 | 2.20 |
| 10 | 2.451 | 2.38 |

scaling in ESS subsumes part of the dissipation region as well. For the latter, the exponents are higher than for the inertial range. It is difficult to say whether the asymptotic value at high Reynolds numbers is the same for shear flows and isotropic turbulence, but such differences as might exist are not large. Finally, according to the refined similarity hypothesis,[19] the difference $2 - \zeta_6$ is the so-called intermittency exponent. In the asymptotic regime, $2 - \zeta_6$ is indeed equal to the intermittency exponent determined independently.[20]

The second point is that we have used the ×-wire data to measure the transverse exponents (i.e., the exponents for the increments of transverse velocity component separated in the longitudinal direction). The high Reynolds number of the present measurements allows us to determine them with enough confidence to say that they are measurably smaller than the longitudinal exponents.[21] The implications of this result have been discussed in Ref. 22), and are outside the scope of this article.

Finally, it should be pointed out that there may be better quantities than structure functions[23] if the scaling properties are the focus. This consideration is also outside the scope of the present work.

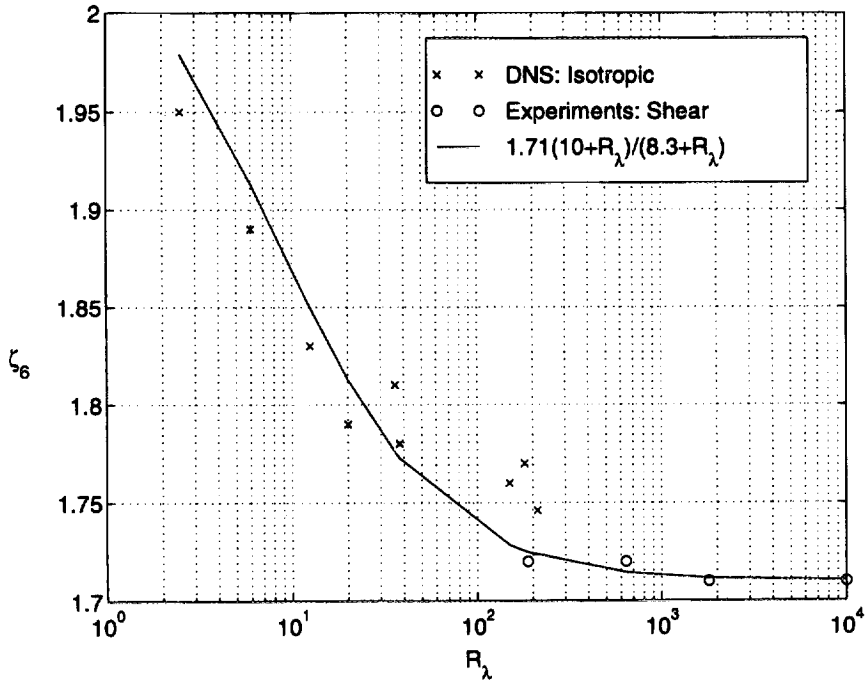


Fig. 12. The $R_\lambda$-dependence of the sixth-order ESS exponent. Data from both isotropic turbulence (DNS) and shear-flow turbulence (experiment) are presented. The DNS sources are: Camussi and Guj,[24] $(R_\lambda, \zeta_6)$ = (2.5, 1.95), (6.0, 1.89), (12.5, 1.83), (20, 1.79), (36, 1.81); Benzi et al.,[11] (38, 1.78); Briscolini et al.,[25] (38, 1.78); Vincenti and Meneguzzi,[26] (150, 1.76); Chen et al.,[22] (181, 1.77), (212, 1.746). Experimental data: Taylor-Couette flow[27], (188, 1.72) and (640, 1.72); present atmospheric data, (10,340, 1.71). The line is a convenient interpolation formula for the data.

## Acknowledgments

We are grateful to Y. Tsuji and V. Cassella for their help with atmospheric measurements, and to S. Chen, M. Nelkin and I. Procaccia for useful discussions. We especially thank Dr. S. Chen for permission to use Fig. 6(a). The work was supported by the NSF grant DMR-9529609.

### References

1) A. N. Kolmogorov, Dokl. Akad. Nauk. SSSR **30** (1941), 299.
2) A. N. Kolmogorov, Dokl. Akad. Nauk. SSSR **32** (1941), 19.
3) U. Frisch, *Turbulence: The Legacy of A.N. Kolmogorov* (Cambridge University Press, Cambridge, 1995).
4) K. R. Sreenivasan and R. A. Antonia, Annu. Rev. Fluid Mech. **29** (1997), 435.
5) K. R. Sreenivasan and B. Dhruva, in preparation.
6) F. Anselmet, Y. Gagne, E. J. Hopfinger and R. A. Antonia, J. Fluid Mech. **140** (1983), 63.
7) P. Tabeling, G. Zocchi, F. Belin, J. Maurer and H. Willaime, Phys. Rev. **E53** (1996), 1613.
8) L. Zubair, "Studies in turbulence using wavelet transforms for data compression and scale separation", Ph.D. Thesis, Yale University, New Haven, CT.

9) G. K. Batchelor, Proc. Camb. Phil. Soc. **47** (1951), 359.
H. Effinger and S. Grossmann, Z. Phys. **B66** (1987), 289.
L. Sirovich, L. Smith and V. Yakhot, Phys. Rev. Lett. **72** (1994), 344.
10) G. Stolovitzky, K. R. Sreenivasan and A. Juneja, Phys. Rev. **E48** (1993), R3217.
11) R. Benzi, S. Ciliberto, R. Tripiccione, C. Baudet, F. Massaioli and S. Succi, Phys. Rev. **E48** (1993), R29.
12) G. Stolovitzky and K. R. Sreenivasan, Phys. Rev. **E48** (1993), R33.
13) H. L. Grant, R. W. Stewart and A. Moilliet, J. Fluid Mech. **12** (1962), 241.
F. H. Champagne, J. Fluid Mech. **86** (1978), 67.
14) S. Chen, G. D. Doolen, R. H. Kraichnan and Z.-S. She, Phys. Fluids **A5** (1993), 458.
15) A. A. Praskovsky, E. B. Gledzer, M. Yu. Karyakin and Y. Zhou, J. Fluid Mech. **248** (1993), 493.
K. R. Sreenivasan and G. Stolovitzky, Phys. Rev. Lett. **77** (1996), 2218.
16) C. Meneveau, Phys. Rev. **E54** (1996), 3657.
17) N. Cao, S. Chen and Z.-S. She, Phys. Rev. Lett. **76** (1996), 3711.
18) N. Cao, S. Chen and K. R. Sreenivasan, Phys. Rev. Lett. **77** (1996), 3799.
19) A. N. Kolmogorov, J. Fluid Mech. **13** (1962), 82.
20) K. R. Sreenivasan and P. Kailasnath, Phys. Fluids **A5** (1993), 512.
21) B. Dhruva, Y. Tsuji and K. R. Sreenivasan, Phys. Rev. **E56** (1997), 4928.
22) S. Chen, K. R. Sreenivasan and M. Nelkin, Phys. Rev. Lett. **79** (1997), 2253.
23) V. S. L'vov and I. Procaccia, Phys. Rev. Lett. **76** (1996), 2896.
K. R. Sreenivasan, A. Juneja and A. K. Suri, Phys. Rev. Lett. **75** (1995), 433.
24) R. Camussi and G. Guj, Experiments in Fluids **20** (1996), 199.
25) M. Briscolini, P. Santangelo, S. Succi and R. Benzi, Phys. Rev. **E50** (1994), 1745.
26) A. Vincent and M. Meneguzzi, J. Fluid Mech. **225** (1991), 1.
27) G. S. Lewis, "Velocity fluctuations, wall shear stress and the transition in torque scaling at R = 13,000 in turbulent Couette-Taylor flow", Ph.D. Thesis, U. Texas at Austin, 1996.